Environ. Sci. Technol. **2002**, *36,* 769−777

Transport of Silica Colloids through Unsaturated Porous Media: Experimental Results and Model Comparisons

JOHN J. LENHART AND JAMES E. SAIERS*

School of Forestry and Environmental Studies, Yale University, 370 Prospect Street, Greeley Laboratory, New Haven, Connecticut 06511

We present results on the migration of silica colloids through laboratory columns packed with partially saturated quartz sand. The transport of the silica colloids responds to changes in the steady-state volumetric moisture content (Θ) and for low Θ depends on the wetting history of the sand pack prior to colloid injection. A mathematical model that incorporates a first-order rate law to simulate film straining and a second-order rate law to simulate partitioning at air−water interfaces closely describes colloid transport and mass transfer over the range of experimental conditions tested. The mass-transfer parameters of the model are sensitive to changes in both the level of water saturation and the flow rate. A semiempirical expression, based on a modification of film-straining theory, accounts for the observed variation in the first-order rate coefficient with changes in Θ and average porewater velocity. Our work indicates that the presence of the air phase substantially influences porewater concentrations of mineral colloids in water-unsaturated media and that the kinetics of particle removal attributed to air−water boundaries reflects the contribution of multiple mass-transfer mechanisms.

Introduction

Large concentrations of colloids are mobilized within the vadose zone during infiltration events (*1*−*5*). These microscopic particles can bind a variety of dissolved contaminants (*6*, *7*), and thus contaminant fluxes above and across the water table may depend heavily on colloid mobility (*8*, *9*). Advection and dispersion, together with mass-transfer reactions that add or remove colloids from the porewater, govern the transport and distribution of colloids in vadose-zone environments.

Mass-transfer reactions at both solid−water and air−water interfaces influence mobile-phase colloid concentrations in partially saturated porous media. Interactions at the solid−water interface have been studied intensively in water-saturated systems (*10*−*13*); however, comparatively few studies have focused on analysis of solid−water or air−water interface mass-transfer reactions in water-unsaturated systems. Wan and Wilson (*14*) constructed glass micromodels to examine colloid movement through pores filled with air and water and demonstrated that hydrophobic and hydrophilic colloids are retained irreversibly at the air−water interface (see Plates 1 and 2 in ref *14*). These results are consistent with breakthrough data on the transport of latex microspheres through partially saturated sand columns (*15*) and form the basis for a mathematical model incorporating advective−dispersive transport, second-order rate-limited colloid capture at air−water interfaces, and first-order kinetics deposition at solid−water interfaces (*16*). More recently, Wan and Tokunaga (*17*) reported that hydrophilic latex colloids are retained in sand packs when the moisture content falls below a threshold value, adjacent pendular rings (i.e., water held by surface tension near the contact point of mineral grains) disconnect, and the films of water that surround the mineral grains become too thin to effectively transmit colloids (see Figures 1 and 2, p 2414, in ref *17*). Wan and Tokunaga (*17*) quantified the kinetics of this film straining with a first-order irreversible rate law.

Volumetric moisture content and porewater velocity (which is a function of the hydraulic conductivity and the gradient in capillary pressure head) play a key role in colloid mass transfer with the air phase. In unsaturated systems, the relationships between moisture content, capillary pressure head, and hydraulic conductivity are complex and depend on whether the soil is imbibing (wetting) or drying (*18, 19*). For example, the moisture content at a given capillary pressure is greater during imbibition than during drainage. Owing to hysteresis in hydraulic properties, mass-transfer reactions may depend on the wetting history of the porous media, thereby substantially complicating descriptions of colloid transport through the vadose zone. Despite its potential importance, the influence of wetting history on colloid mobility remains unexplored.

A comprehensive theory for colloid transport that takes into account the unique complexities associated with vadose-zone environments awaits development. Mathematical models for colloid transport and mass transport in unsaturated media have been formulated [i.e., those of Corapcioglu and Choi (*16*) and Wan and Tokunaga (*17*)], but these models have not been widely tested. The dearth of model evaluations reflects the proportionate scarcity of experimental data appropriate for testing the models. Several published data sets demonstrate the general trend of increasing colloid retention with decreasing moisture content (e.g., refs *15* and *20*); however, in all but a few studies (*20*−*22*), these data were generated in experiments where the moisture content was not monitored with time or over the length of the flow path. This spatial and temporal variability in moisture content complicates model application (see ref *16*) and precludes the derivation of well-constrained relationships between the model coefficients for colloid mass transfer and the water content of the medium.

We report the results of column experiments on the transport of silica colloids through water-saturated and -unsaturated porous media. To isolate the effects of the air phase on colloid deposition kinetics, we packed the column with clean quartz sand, which was chemically treated to minimize colloid attachment at the solid−water interface. A uniform and steady level of water saturation was maintained in each experiment by careful control of the column inflow and outflow rates. Our results demonstrate that colloid breakthrough is sensitive to variation in moisture content and, for low moisture contents, depends on the wetting history of the sand beds prior to the period of colloid injection. We also find that a transport model, modified to account for both first-order and second-order colloid mass-transfer reactions, describes colloid breakthrough more closely than

* Corresponding author phone: (203)432-5121; fax: (203)432-3929; e-mail: james.saiers@yale.edu.

10.1021/es0109949 CCC: $22.00
Published on Web 01/08/2002

TABLE 1. Summary of Experimental Conditions and Model Results

						R^2 values			best-fit parametervalues[a] (dual rate-law model)			theor. values[b]
expt	Θ	Ψ (cm of H_2O)	wetting history[c]	v (cm/h)	A_L (cm)	first-order	second-order	dual rate	k_1 (h^{-1})	k_2 (h^{-1})	X (mg/L)	k_1 (h^{-1})
SAT1	0.384			12.6	0.061							
SAT2	0.383			12.0	0.074							
UNSAT1A	0.168	−25.7	D	117	0.91							
UNSAT1B	0.166	−27.2	D	119	0.90	0.9917	0.9961	0.9963	0.158 (0.021)	0.427 (0.037)	10.00 (1.98)	0.158
UNSAT2A	0.121	−28.7	D	38.7	0.61							
UNSAT2B	0.118	−29.2	D	39.0	0.61	0.9453	0.9899	0.9983	0.131 (0.0019)	0.485 (0.0075)	20.37 (0.42)	0.127
UNSAT2C	0.119	−18.5	I	35.0	0.54							
UNSAT2D	0.118	−18.5	I	24.3	0.78	0.9501	0.9883	0.9963	0.109 (0.0026)	0.346 (0.0099)	18.40 (0.72)	0.111
UNSAT3A	0.089	−30.2	D	12.6	0.81							
UNSAT3B	0.085	−30.0	D	13.3	0.76	0.8856	0.9684	0.9947	0.079 (0.0010)	0.249 (0.0051)	20.05 (0.47)	0.09
UNSAT3C	0.090	−22.4	I	7.26	0.82							
UNSAT3D	0.087	−22.9	I	8.88	0.67	0.8876	0.9749	0.9977	0.080 (0.0006)	0.159 (0.0021)	19.77 (0.35)	0.07

[a] Data sets from duplicate experiments were used simultaneously in each inversion, so a single parameter set was identified for each experimental treatment. Standard errors of the parameter estimates of the dual rate-law model are given in parentheses beneath the optimal parameter value. [b] Theoretical values of k_1 were calculated from eq 7 using measurements of Θ and v averaged from duplicate experiments. [c] Wetting history refers to the method in which the target moisture content was attained, either by drying (D) or by imbibing (I).

single rate-law models and that the governing parameters of this dual rate-law model vary in a discernible fashion with moisture content.

Experimental Methods

Overview. We measured colloid and bromide transport under saturated conditions and at three moisture contents below saturation (Table 1). These experiments were conducted in duplicate under conditions of steady and uniform flow. We examined the effects of wetting history by employing two different methods to attain the target saturation. The drying method involved slowly draining a saturated sand column to the target moisture content, while the imbibing method involved drying a saturated sand pack to near its residual moisture content and then immediately rewetting the column to reach its target moisture content. Once the column had stabilized at its target moisture content, bromide (a conservative tracer) and silica colloids were applied sequentially to the column. The drying method was used in three sets of unsaturated experiments (UNSAT1A, -1B, -2A, -2B, -3A, and -3B) to achieve moisture contents of 0.17, 0.12, and 0.09. The imbibing method was employed in two sets of experiments (UNSAT2C, -2D, -3C, and -3D) to achieve moisture contents of 0.12 and 0.09 (Table 1).

Preparation of Materials. Spherical silica particles (MP-3040, Nissan Chemical Industries Ltd.) were used as the colloidal phase in all experiments. The diameter of these particles, as measured by dynamic light scattering (Zeta-Pals Analyzer, Brookhaven Instruments), equaled 360 ± 4 nm; their density equaled 2.28 g/cm^3. Suspensions of the silica colloids were prepared by diluting aliquots of a concentrated stock with a dilute electrolyte solution to achieve a colloid concentration of 100 mg/L. The electrolyte solution consisted of 0.84 mM NaCl and 0.16 mM $NaHCO_3$ in deionized water (E-Pure, Barnstead/Nanopure) and had a pH and ionic strength of 7.4 and 0.001 M, respectively.

Well-rounded quartz sand was used as the porous medium (Accusand 40/60, Unimin Corp.). Using stainless steel sieves and a sieve shaker (RX-29 Ro-Tap, W. S. Tyler), we isolated the fraction of sand with a size between 300 and 355 μm for use in the column experiments. As received from the distributor, the surfaces of the quartz grains are coated with metal oxides (Fe, Al, and Ti) and trace quantities of organics. These impurities may influence surface charge characteristics of the sand and may promote colloid deposition (*23*). We removed the surface coatings by chemically treating the sand following a modification of a procedure developed by Kohler et al. (*24*). After the sieved sand was rinsed several times in deionized water to remove colloid-sized particles, the sand was boiled in 50% concentrated HNO_3 for 2 h to dissolve iron and aluminum oxides and to oxidize organics. The acid was decanted, and the solids were repeatedly rinsed with deionized water until the pH stabilized at a near-neutral value. Amorphous silica and remaining colloids were removed by agitating the sand in 0.002 N NaOH for 2 h on a horizontal shaker table at 150 oscillations per minute. The basic solution was decanted, and the solids were rinsed thoroughly with deionized water before treating the sand with 0.001 M HNO_3 for 12−14 h to remove any remaining cations. Following the acid wash, the sand was rinsed with deionized water until the pH approached 7, and then it was dried at 110 °C.

Unsaturated Column Experiments. The cleaned quartz sand was packed in acrylic columns with an internal diameter and length of 12.7 and 32.8 cm, respectively (Figure 1). Porous frit assemblies, used to support the sand and to disperse the influent solution, were fabricated from 1/8-in.-thick polypropylene disks (Porex Co., Inc) with 120 μm pores. These disks were bonded to stainless steel rings with a two-part urethane adhesive (Durabond U-05FL, Loctite Corp.). Capillary pressure within the column was maintained by nylon membranes with 20 μm pores (Spectra/Mesh, Spectrum Laboratories, Inc.). The membranes were placed in immediate contact with the polypropylene porous frit assemblies, and each assembly was sealed in the column using two butyl rubber O-rings. To allow air to escape the column, six vent holes were drilled on opposite sides at 2.1, 16.4, and 30.7 cm from the top of the vertically oriented column. The venting holes were sealed with gas-permeable porous PTFE membranes (Milliseal Disk, Millipore) to prevent loss of water or sand from the column. Results of preliminary experiments (performed without the sand) demonstrated that neither the acrylic column nor the end-fitting assemblies removed silica colloids from suspension.

Both volumetric moisture content and capillary pressure head were measured at 7.7, 16.4, and 25.1 cm from the top of the column. Probes sensitive to changes in the apparent dielectric constant of the sand pack (ML2x Thetaprobe, Delta-T Devices, Ltd.) were used to monitor the volumetric moisture content. Capillary pressure head was measured with tensiometers that were constructed according to the design of Eching and Hopmans (*25*) with high-flow ceramic cup-tube assemblies (2100-200CR-B1M3, Soil Moisture, Corp) and differential microtransducers (26PCAFA6D, Honeywell/Microswitch). Data from the tensiometers and the moisture-

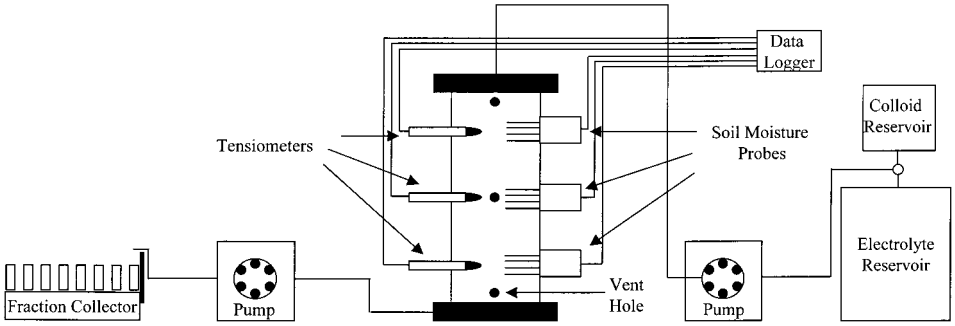

FIGURE 1. Schematic of the laboratory columns used in the experiments on colloid transport.

content probes were collected continuously using a datalogger (DL2e, Delta-T Devices, Ltd.). The tensiometers were calibrated to an accuracy of ±3% and a precision of 0.2 cm using a falling head manometer. Prior to each experiment, the soil moisture probes were calibrated according to the manufacturer using the readings from oven-dried and saturated sand samples. These two readings varied by less than 0.5% between experiments. Using this method of calibration, the manufacturer reports that the soil moisture probes are accurate to ±1%. For our system, we determined the precision of the probes to be 0.001 m^3/m^3.

For each experiment, a fresh column was packed by pouring sand in 250-g increments into a small volume of the electrolyte solution standing in the column. After each increment of sand, the contents of the column were stirred using a polypropylene stir-rod and the sides of the column were tapped a uniform number of times. A total of 7180 ± 20 g of sand was used in each experiment. The average porosity of the sand pack, determined from measurements of the saturated column pore volume, equaled 0.338 ± 0.002.

Water and colloids were applied to the top of the column using a peristaltic pump equipped with a six-roller cartridge pump head and Tygon LFL tubing (all Cole-Parmer Instrument, Co.). An identical pump was used to extract solutions from the base of the column. Two approaches were used to achieve the desired level of water saturation. The drying method consisted of draining an initially saturated sand column to the target moisture content. The imbibing method involved draining a saturated column to near the residual moisture content (≈0.045) before immediately rewetting the column to the desired level of saturation. In both types of experiments, a unit hydraulic head gradient was established after the equilibration period by setting the inflow rate equal to the outflow rate. Once the effluent pH matched the influent pH and the moisture content and capillary pressure stabilized at the target values, a solution containing 0.50 mM NaBr, 0.84 mM NaCl, and 0.16 mM $NaHCO_3$ was introduced into the top of the column. Water samples were collected from the base of the column in polypropylene test tubes with a fraction collector (IS-95, Spectrum Chromatography Inc.) and analyzed for bromide concentrations using an ion-selective electrode (Cole Parmer). Following application of a 2.1-L bromide pulse, bromide-free NaCl/$NaHCO_3$ was applied until bromide concentrations in the column effluent returned to zero. Once the column was thoroughly flushed of bromide, a 100 mg/L suspension of silica colloids (prepared as described above) was applied to the column as a step input. Effluent samples were collected at regular intervals and analyzed for colloid concentrations by measuring the total extinction of light at a wavelength of 350 nm with an UV/visible spectrophotometer (DU 520, Beckman). Light extinction measurements made on effluent samples collected prior to the colloid injection were identical to those of filtered water, indicating that particle mobilization from the quartz sand was negligible.

Saturated Column Experiments. Experiments on the transport of bromide and silica colloids through saturated media were conducted following the methods outlined by Saiers and Hornberger (*26*). Glass chromatography columns with an internal diameter of 4.8 cm were used to contain the sand, and a single peristaltic pump, located at the base of the vertically oriented columns, controlled the flow of water, solutes, and colloids through the columns. These experiments were conducted with the same type of sand and under the same chemical conditions as the experiments in unsaturated media.

Theory

Model for Colloid Transport in Unsaturated Media. We present the equations for a mathematical model that couples advective−dispersive transport with rate-limited mass-transfer reactions for particle retention within partially saturated sand columns. In our experiments, the deposition of silica colloids onto the thoroughly cleaned quartz sand was negligible, and colloid mass transfer was controlled solely by the presence of the air phase. Water flow in our unsaturated columns occurred simultaneously through films of water adsorbed to the sand grains, narrow water-filled pores, and connected pendular rings (*18*, *27*). On the basis of this conceptualization of the flow domain, we assume that straining of colloids within thin films of adsorbed water and sequestration of colloids that diffuse to immobile air−water interfaces remove colloids from mobile phase.

The one-dimensional form of the advection−dispersion equation describes the movement of colloids in our sand columns:

$$\frac{\partial C}{\partial t} + \frac{\rho_b}{\Theta}\frac{\partial S_F}{\partial t} + \frac{\Theta_A}{\Theta}\frac{\partial S_{AW}}{\partial t} = \frac{qA_L}{\Theta}\frac{\partial^2 C}{\partial z^2} - \frac{q}{\Theta}\frac{\partial C}{\partial z} \qquad (1)$$

where C is the porewater colloid concentration (colloid mass per liter of porewater), t is time, ρ_b is the bulk density, Θ is the volumetric moisture content, S_F is the concentration of colloids trapped within thin films (mass of colloids per gram of sand), Θ_A is the volumetric air content ($\Theta_A = n - \Theta$, where n equals porosity), S_{AW} is the concentration of colloids associated with the air−water interface (mass of colloids per liter of air), A_L is the longitudinal dispersivity, z is the coordinate parallel to flow, and q is the specific discharge. Equation 1 is coupled with two rate laws that quantify temporal changes in concentrations of colloids within thin-water films and at air−water interfaces.

According to Wan and Tokunaga (*17*), colloid immobilization by film straining depends, in part, on the probability of pendular ring discontinuity and on the ratio of colloid size to film thickness. The probability of pendular ring discontinuity varies inversely with moisture content; in other words, the fraction of disconnected pendular rings increases from zero to unity as Θ decreases from its saturated value (i.e., $\Theta = n$) to its residual value (i.e., $\Theta = \Theta_r$, where Θ_r is the residual

moisture content). As pendular rings disconnect, an increasing proportion of water flow and colloid transport is relegated to the adsorbed films of water that envelop the mineral grains. When film width is greater than colloid diameter, straining remains ineffective; however, when film width is similar to or less than the colloid diameter, surface tension retains colloids against the mineral grain surfaces. Once trapped within thin films, particle escape does not occur unless the films expand owing to an increase in volumetric moisture content. A first-order rate law quantifies the temporal change in concentrations of colloids immobilized within thin films (*17*):

$$\frac{\rho_b}{\Theta}\frac{\partial S_F}{\partial t} = k_1 C \tag{2}$$

where k_1 is a first-order rate coefficient. Values of k_1 can be calculated from information on pendular ring discontinuity, film thickness, and flow rate (*17*):

$$k_1 = P(\Psi)\left(\frac{d}{w}\right)^{\beta} N v^{(1+h)} \tag{3}$$

where $P(\Psi)$ is the probability of pendular ring discontinuity (expressed as a function of capillary pressure head, Ψ); d is the colloid diameter; w is the film thickness; and h, N, and β are empirical parameters [that Wan and Tokunaga (*17*) presumed constant for geometrically similar media]. The film thickness is a function of Ψ and can be calculated from (*28*)

$$w = \sqrt[3]{\frac{A_{svl}}{6\pi\rho g\Psi}} \tag{4}$$

where A_{svl} is the Hamaker constant for solid−vapor interaction through the intervening liquid, ρ is the density of water, and g is the acceleration due to gravity. According to the theory of thin films, the formation of a thermodynamically stable wetting film requires that A_{svl} be negative in sign (*29*).

In addition to colloid retention within thin films of adsorbed water, colloids traveling within relatively large water channels and through connected pendular rings may diffuse to the air−water interface where they are captured by capillary forces. Wan and Wilson (*14*) reported that the affinity of colloids for the air−water interface increases with particle hydrophobicity and that, once deposited, both hydrophobic and hydrophilic colloids are thermodynamically stable at the interface, irreversibly held by surface tension (*30*). Following Corapcioglu and Choi (*16*), we assume that the kinetics of this air−water interface reaction depend on the porewater colloid concentration and on the fraction of air−water interface available to scavenge particles, such that

$$\frac{\Theta_A}{\Theta}\frac{\partial S_{AW}}{\partial t} = k_2\frac{X - S_{AW}}{X}C \tag{5}$$

where k_2 is a rate coefficient and X is the retention capacity of the air−water interface (mass of colloids retained per liter of air). Second-order rate laws of the form of eq 5 have been used successfully to describe the deposition of inorganic colloids in saturated systems for conditions in which colloids and collectors possess opposite surface charges (*31*) and more recently to describe deposition kinetics of latex microspheres, viruses, and bacteria in unsaturated systems (*16*, *21*, *22*).

Equations 1, 2, and 5 are appropriate for describing the one-dimensional transport of colloids through unsaturated media for cases in which colloid mass transfer is dominated by reactions within thin-water films and at immobile air−water interfaces. We solved eqs 1, 2, and 5 by using a finite-difference method with a predictor−corrector time-stepping scheme for zero initial concentrations, a first-type upper boundary condition, and a zero gradient in concentration at the column base. We used the breakthrough data on silica transport to test this dual rate-law model as well as to test two simplified versions, referred to as the first- and the second-order models. The first-order model, governed by eqs 1 and 2, is consistent with the equations presented by Wan and Tokunaga (*17*) for transport and film-straining, while the second-order model, governed by eqs 1 and 5, is consistent with equations presented by Corapcioglu and Choi (*16*) for transport and air−water interface capture.

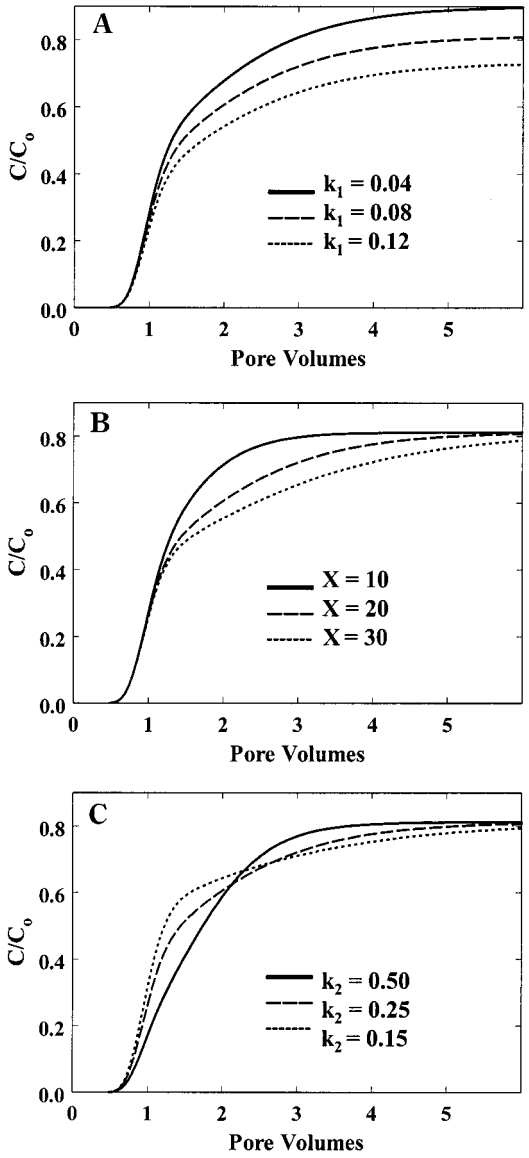

FIGURE 2. Sensitivity of colloid breakthrough (as calculated by the dual rate-law model) to variation in (A) k_1, (B) X, and (C) k_2.

Sensitivity Analysis. We examined the response of colloid breakthrough, as calculated by the dual rate-law model, to changes in the values of k_1, k_2, and X. Sensitivity analyses with first- and second-order single rate-law models are published elsewhere and will not be reproduced here (*16*, *31*). In a sequence of nine simulations, the values of k_1, k_2, and X were varied independently about their base-case values of 0.08 h^{-1}, 0.25 h^{-1}, and 20 mg/L, respectively, while the values of C_0, n, Θ, v, and A_L were fixed at 100 mg/L, 0.34, 0.09, 12.6 cm/h, and 0.8 cm, respectively.

The value of k_1 (the rate coefficient in eq 2) controls the magnitude of the peak breakthrough concentrations; that is, as k_1 increases from 0.04 to 0.12 h^{-1}, steady-state effluent

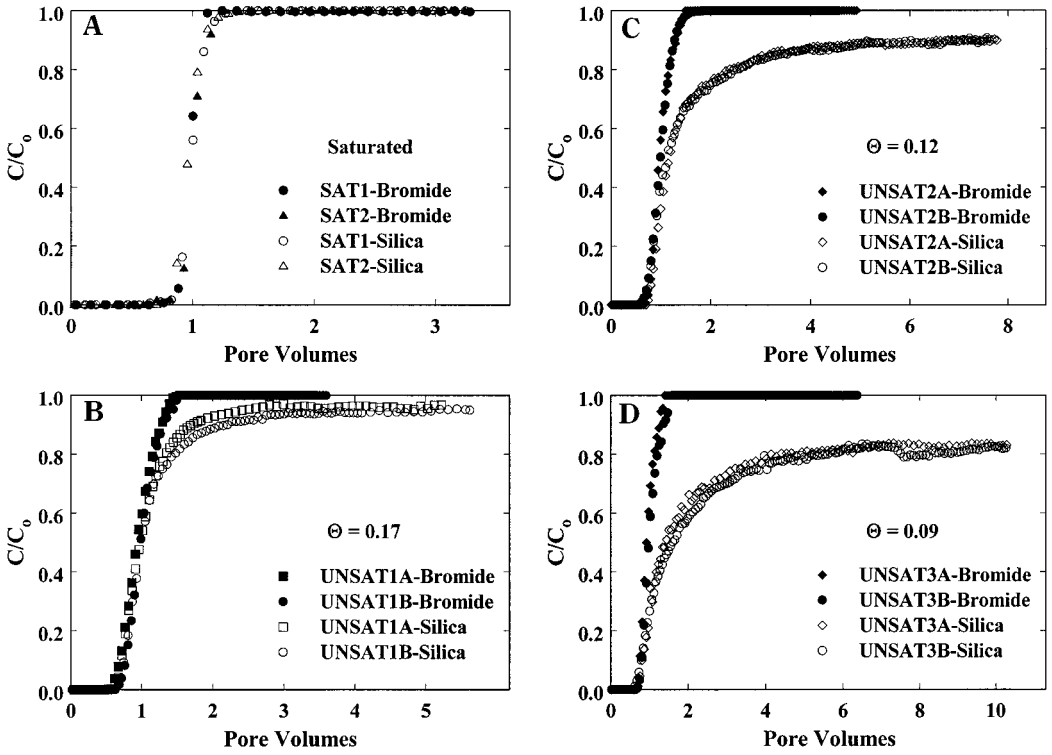

FIGURE 3. Bromide and silica breakthrough curves for experiments conducted at (A) saturation and steady-state moisture contents of (B) 0.17, (C) 0.12, and (D) 0.09. The experiments conducted at saturated conditions utilized a 4.8 cm diameter glass column; the remaining experiments employed a 12.7 cm diameter acrylic column. The breakthrough curves were measured in columns preequilibrated by drying. A pore volume equals $qtlL\Theta$, where L is the column length.

concentrations decline from $C/C_0 = 0.9$ to $C/C_0 = 0.7$ (Figure 2A). Steady-state breakthrough is not achieved until the capacity of the air−water interfaces to bind colloids is exhausted (i.e., $X = S_{AW}$ in eq 5), and hence, the time to stable peak concentrations increases as X increases from 20 to 30 mg/L (Figure 2B). Colloid deposition at air−water interfaces is governed by k_2 (the rate coefficient in eq 5) as well as by X. For a fixed value of X, increases in k_2 lead to more rapid colloid saturation of the air−water interfaces, which in turn decreases the time required for effluent concentrations to stabilize at maximum levels (Figure 2C).

Results and Discussion

Close reproducibility of the experiments on the transport of bromide and silica colloids relied on careful control and monitoring of the flow conditions. We maintained spatially uniform and steady volumetric moisture content (Θ) and capillary pressure head (Ψ) during each experiment by balancing column inflow and outflow rates. For any given time following column equilibration, the difference in Θ between the top and the bottom moisture probes did not exceed 5% of the average of the moisture contents measured at all three moisture probes. Temporal variation in Θ at each of the three moisture-probe locations was less than ±1.5%, except in experiments UNSAT2A and -3B, where Θ at the bottom sensor varied by ±4% and ±2.4%, respectively. The time-averaged values of Θ for each sensor were averaged to give an effective column Θ, which was used as input in the colloid transport model (Table 1). Temporal and spatial variations in Ψ were similarly small, and effective column values of Ψ were determined in the same way as those for Θ. Values of Ψ were greater (less negative) in the imbibing experiments than in the corresponding drying experiments conducted at the same Θ, reflecting the expected hysteresis in the $\Theta-\Psi$ relationship (Table 1).

The breakthrough curves on colloid transport through the saturated columns match those of bromide (Figure 3A), indicating that mass-transfer reactions at solid−water interfaces did not remove measurable quantities of silica colloids from porewater suspension. Strong repulsive forces between the negatively charged silica colloids and quartz sand inhibited deposition. The silica colloids should exhibit the same weak affinity for the quartz sand in the unsaturated experiments because both the saturated and the unsaturated experiments were conducted under identical chemical conditions.

Colloid mobility within the partially saturated sand packs was high, with peak breakthrough concentrations reaching at least $C/C_0 = 0.75$ in all experiments (Figure 3B−D). The transport of silica colloids was not conservative however. Steady-state breakthrough concentrations decreased with decreasing Θ, indicating that the mass of colloids retained in the column varied inversely with the level of water saturation. These findings are in agreement with observations on the transport of latex microspheres, bacteria, and viruses through unsaturated sand (*15*, *20*−*22*, *32*).

Our experiments indicate that the functional relationships between Θ, Ψ, and hydraulic conductivity (K) depend on the wetting and the drying history of the porous media (Figure 4A,B). We find that these hysteretic relationships between hydraulic parameters can, under some conditions, lead to nonunique relationships between Θ and the breakthrough of silica colloids (Figure 5A,B). In experiments conducted at $\Theta = 0.09$, the porewater velocity (v) was on average 38% lower (owing to the dependence of K on wetting history, as shown in Figure 4B), and colloid retention within the columns was on average 10% greater in experiments that employed the imbibing method as compared to experiments that employed the drying method (Figure 5A). The porewater velocities varied by less than 10% in three of the four experiments at $\Theta = 0.12$ (UNSAT2A, UNSAT2B, and UNSAT2C), which resulted in three nearly identical colloid breakthrough curves (Figure 5B). Flow rates were poorly reproduced in the imbibing experiments at $\Theta = 0.12$

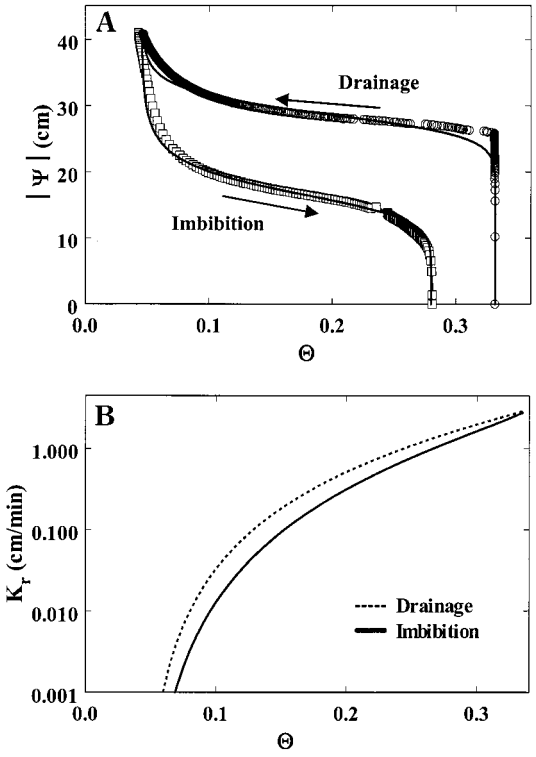

FIGURE 4. (A) Characteristic curves for the quartz sand measured during drainage (open circles) and imbibition (open squares) and characteristic curves calculated by fitting eq 21 from van Genuchten (*19*) to the data (solid lines). (B) Variation in relative hydraulic conductivity computed for drainage (dashed line) and imbibition (solid line) using parameters estimated from the moisture characteristics curves and eq 8 of van Genuchten (*19*). Relative hydraulic conductivity, K_r, equals $K(\Theta)/K_{sat}$, where $K(\Theta)$ is the moisture-content-dependent hydraulic conductivity and K_{sat} is the hydraulic conductivity of the saturated media. Flow was uniform in our experiments, so $d\Psi/dz = 0$ and by Darcy's equation, $q = K(\Theta)$.

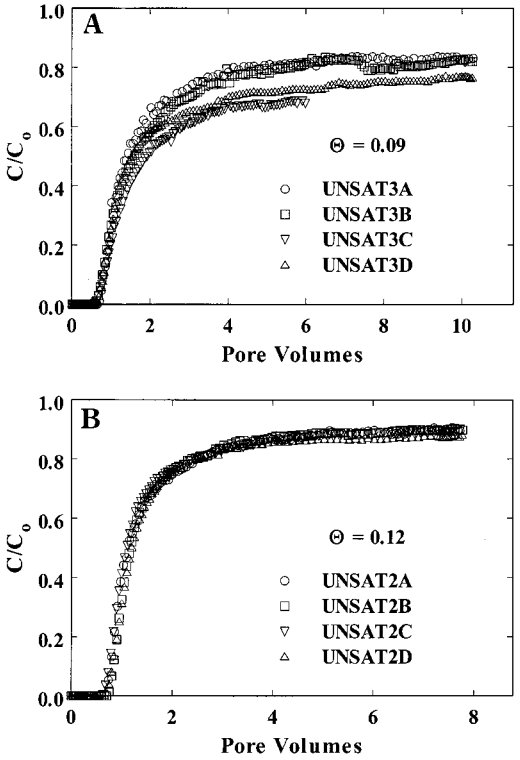

FIGURE 5. Measured silica breakthrough curves for imbibing- and drying-type experiments conducted at volumetric moisture contents of (A) 0.09 and (B) 0.12. In imbibing-type experiments, a sand column at near its residual moisture content was imbibed to the target moisture content, while in drying-type experiments, an initially saturated sand column was drained to its target moisture content.

(UNSAT2C and UNSAT2D), and only in UNSAT2D, where the porewater velocity was 37% lower than in the drying experiments (UNSAT2A and UNSAT2B), were the anticipated effects of hysteresis in the $K-\Theta$ relationship on porewater velocity observed. Despite the substantial flow-rate reduction in UNSAT2D, peak effluent concentrations of colloids declined by only 3% (Figure 5B), results which suggest that the dependence of colloid breakthrough on porewater velocity is weaker in experiments at $\Theta = 0.12$ than in experiments at $\Theta = 0.09$.

We evaluated the kinetics of colloid mass transfer by comparing experimental breakthrough curves to those calculated by the first-order model (eqs 1 and 2), the second-order model (eqs 1 and 5), and the dual rate-law model (eqs 1, 2, and 5). Optimal values of the mass-transfer parameters were identified by using the Levenberg−Marquardt least-squares algorithm to minimize an objective function, defined as the sum of the squared residuals between model-calculated and measured breakthrough concentrations. Measured concentrations from duplicate experiments were used simultaneously in each least-squares inversion in order to identify a single parameter set for each experimental treatment. We obtained estimates of dispersivity required to run the silica transport simulations by fitting solutions of the standard advection−dispersion equation to the data on bromide transport (Table 1).

The single rate-law models account for much of the variation in the experimental data; however, agreement between measured and calculated concentrations worsens progressively as Θ decreases (Figure 6A−C; R^2 values in Table 1). At $\Theta = 0.09$, the driest condition evaluated, the first-order model overestimates effluent concentrations measured prior to maximum breakthrough, while the second-order model fails to reproduce the observed stabilization of breakthrough concentrations (Figure 6C). We performed additional simulations with modified versions of the single rate-law models that accounted for first-order colloid remobilization, but these reversible kinetics formulations did not provide an improved description of the experimental breakthrough curves (simulations not shown). These results are consistent with the contention of others that trapping of colloids within thin films and at air−water interfaces is irreversible under conditions of steady fluid flow and porewater chemistry (*14*, *17*, *30*).

Calculations of the dual rate-law model, which incorporates both first- and second-order formulations, match the breakthrough data from the various experiments nearly exactly (Figure 6D−F). R^2 values for dual rate-law model fits are equal to or exceed 0.995 and, for every experimental treatment, are greater than the corresponding R^2 values for the single rate-law model fits (Table 1). The superiority of the dual rate-law model over the single-rate formulations is especially apparent at low moisture contents, under conditions in which colloid immobilization within the sand packs is the greatest (compare Figure 6, panels C and F). We infer from these results that both thin-film straining and capture at air−water interfaces contribute to colloid immobilization.

We compared the role of the two reaction mechanisms in colloid immobilization by using the dual rate-law model to calculate the mass of colloids associated with the thin films and air−water interfaces at the completion of a 3.5-L injection of the 100 mg/L colloid suspension. The mass of colloids retained at air−water interfaces increased 2-fold as Θ decreased from 0.17 to 0.12 but stabilized at a nearly constant value and was independent of sand-pack wetting

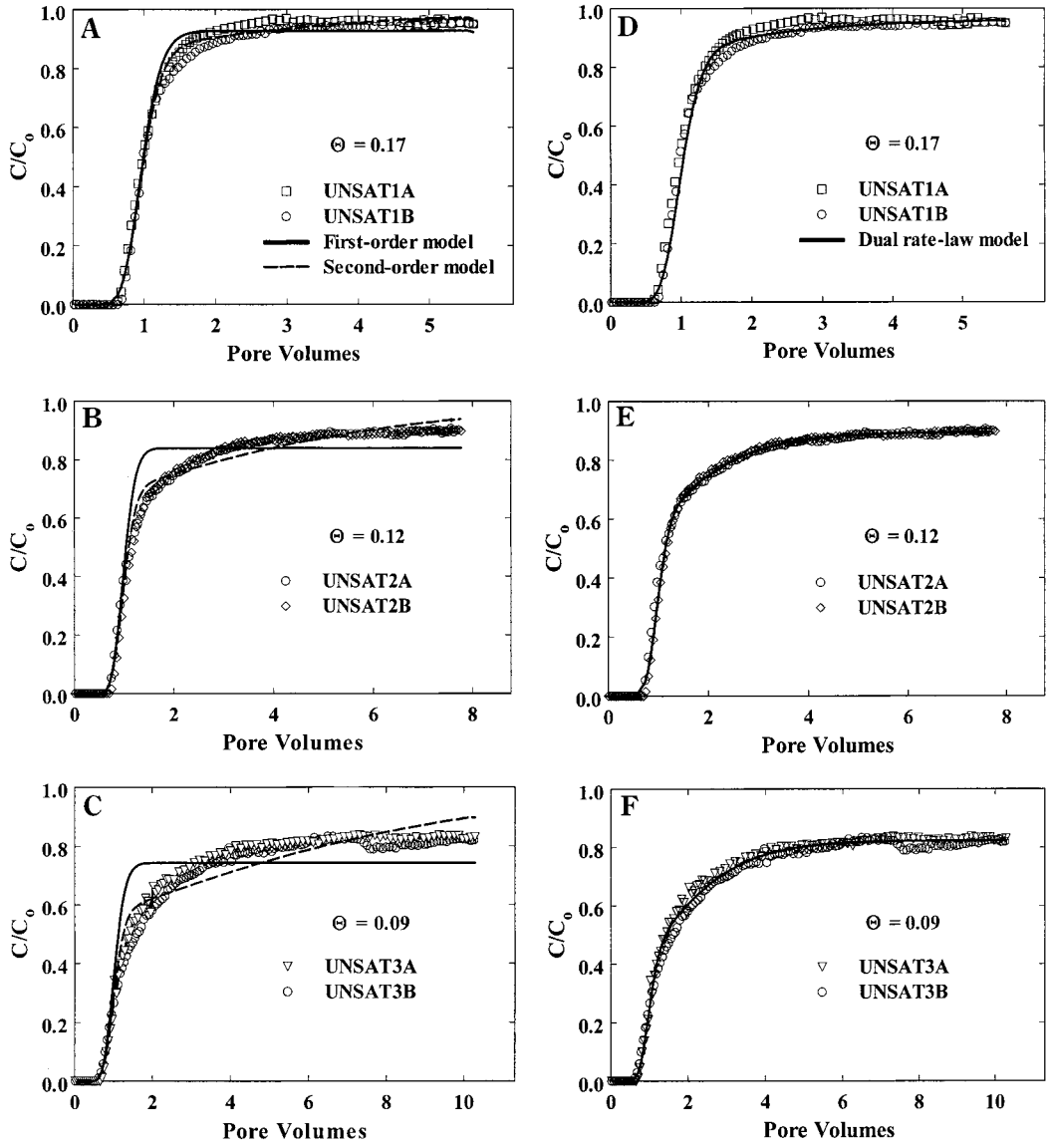

FIGURE 6. Measured silica breakthrough curves (symbols) and breakthrough curves calculated by the first-order model (solid lines in panels A–C), the second-order model (dashed lines in panels A–C), and the dual rate-law model (solid lines in panels D–F). The breakthrough data were measured in experiments in which the columns were preequilibrated by drying.

history for $\Theta \leq 0.12$ (Figure 7). The relative contribution of thin films to total colloid retention varied inversely with volumetric moisture content. At $\Theta = 0.17$, thin films stored approximately half of the colloid mass immobilized within the sand pack (Figure 7). A reduction in Θ to 0.12 promoted more than a 3-fold increase in the mass of silica trapped within thin films, and at $\Theta = 0.09$, film straining accounted for the retention of 70–82% of the total mass of immobilized colloids, depending on wetting history. These results suggest that film straining is an important mechanism over the range of water saturations evaluated here and becomes the dominant mechanism under conditions of intermediate to low moisture contents.

Best-fit estimates of k_1 (the rate coefficient for film straining) of the dual rate-law model vary directly with changes in Θ (Table 1). Calculations based on film-straining theory (i.e., eq 3) predict that, for a given Θ, k_1 will exhibit pronounced sensitivity to wetting history because the capillary pressure head is greater (less negative) when the porous media is equilibrated by imbibing than when its equilibrated by drying (see Figure 4A and Ψ values in Table 1). Such a prediction is counter to our observations; that is, for a particular moisture content, best-fit estimates of k_1 show relatively little variation between imbibing- and drying-type experiments (Table 1).

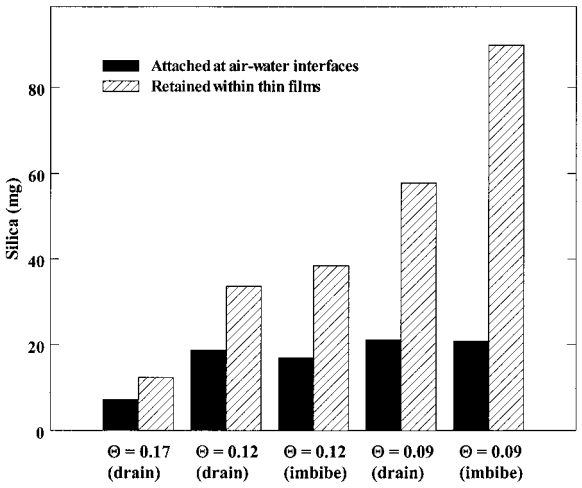

FIGURE 7. Mass of silica retained by film straining and by air–water interface capture, as calculated by the dual rate-law model.

This discrepancy between film-straining theory and observations can be resolved by quantifying the extent of pendular ring disconnectedness in terms of Θ, instead of in terms of Ψ. The key advantage of this approach is that the functional dependence of pendular ring discontinuity on Θ is unaffected by wetting history. Mathematical relationships between pendular ring discontinuity and Θ have been derived for model porous media (e.g., ref *33*); however, these relationships cannot be applied to our experiments owing to nonuniformity in the size, shape, and packing of the quartz sand used to construct the columns. Given the absence of an appropriate pore-scale model for the spatial distribution of water in natural porous media, we assume that the effect of pendular ring disconnectedness on colloid immobilization can be approximated by an empirical function of Θ, $F(\Theta)$, and that k_1 can be expressed by substituting $F(\Theta)$ for $P(\Psi)$ in eq *3*, such that

$$k_1 = F(\Theta)\left(\frac{d}{w}\right)^{\beta} N v^{(1+h)} = \left[1 - \left[\frac{\Theta - \Theta_r}{n - \Theta_r}\right]^{\kappa}\right]\left(\frac{d}{w}\right)^{\beta} N v^{(1+h)} \quad (6)$$

where κ is a constant and Θ_r is the residual moisture content. The function $F(\Theta)$ varies nonlinearly from unity when $\Theta = \Theta_r$ to zero when $\Theta = n$, corresponding to complete pendular ring discontinuity and complete pendular ring connectedness, respectively. Film thicknesses, calculated from eq 4 using a value for A_{svl} of -19×10^{-20} J (*28*), vary from 15.1 to 17.7 nm over the range of pressures studied (Table 1) and are comparable to the values calculated by Wan and Tokunaga (*17*) for a similar range in capillary pressures. This film thickness is much less than the diameter of the silica colloids, and thus all colloids entering thin films will be trapped. Because the term $(d/w)^{\beta}$ is nearly constant across the range of conditions tested here, eq 6 reduces to

$$k_1 = \left[1 - \left[\frac{\Theta - \Theta_r}{n - \Theta_r}\right]^{\kappa}\right] N_2 v^{(1+h)} \quad (7)$$

where N_2, a constant, is equal to $N(d/w)^{\beta}$. For our experimental system then, changes in k_1 are driven by changes in the degree of pendular ring discontinuity and porewater velocity.

We used eq 7 to calculate k_1 for each of the experimental treatments by setting h equal to -0.5, as prescribed by Wan and Tokunaga (*17*), and by optimizing the values of N_2 and κ. We obtained close agreement ($R^2 = 0.95$) between theoretical k_1 values (i.e., those calculated from eq *7*) and measured k_1 values (i.e., those estimated from the silica breakthrough curves) with best-fit values of 0.04 and 0.59 for N_2 and κ, respectively. Theoretical k_1 values fall within 3% of corresponding measured values for the three sets of experiments at $\Theta \geq 0.12$ (Table 1). Discrepancies are greater for the imbibing and drying experiments at $\Theta = 0.09$, but theoretical k_1 values still fall within 14% of measured values. The deviations reveal that the dependence of k_1 on velocity is more complex than depicted by eq 7. While the assumption that k_1 scales proportionately with $v^{0.5}$ is valid for conditions in which Θ equals or exceeds 0.12, it is inappropriate at the lowest moisture content tested. Despite substantial differences in flow rates between the drying and the imbibing experiments at $\Theta = 0.09$, measured k_1 values are nearly identical, indicating that k_1 is essentially independent of v at this moisture content. These results demonstrate that h in eq *7* is not constant but varies as a function of Θ. We are unable to precisely constrain the dependence of k_1 on velocity at this time. Fortunately, in its present form, eq 7 predicts with reasonably good success values of the film-straining coefficient over a 2-fold change in Θ and over an order of magnitude change in v. Furthermore, the modified version of the film-straining formulation circumvents complications associated with hysteresis in the capillary pressure−moisture-content relationship and hence is appropriate for quantifying the magnitude of the film-straining coefficient irrespective of the wetting history of the porous medium.

Given the relatively high mobility of silica colloids in our experiments, we conclude that a substantial fraction of colloids introduced to the columns did not enter into thin films or into dead-end pendular rings but traveled through continuous water ducts with dimensions greater than those of the colloidal particles themselves. Colloids transported within these ducts were free to move to the air−water interface, where, depending on the energy of interaction between the colloids and the interface, capture may have occurred.

Our results show that best-fit values of X (the retention capacity of air−water interface) increase from 10 mg/L at $\Theta = 0.17$ to a stable value of 20 mg/L at $\Theta \leq 0.12$ (Table 1). Differences in flow intensity between the experiments may account for the relationship between X and Θ. According to Ko and Elimelech (*34*), the shear component of fluid flow for colloid Peclet numbers greater than ca. 1 is sufficient to reduce the colloid retention capacity of solid collectors. Colloid Peclet numbers ($= vr_c/D$, where r_c is the colloid radius and D is the Stokes−Einstein diffusion coefficient) range between 0.3 and 1.7 for the six experiments conducted at $\Theta \leq 0.12$, and values of X are nearly constant for these experiments. An increase in Θ from 0.12 to 0.17 promotes a 3-fold increase in the colloid Peclet number to 5.4 and a corresponding 50% decrease in X. These results are in agreement with the theory proposed by Ko and Elimelech (*34*) and suggest that hydrodynamic forces acting near immobile air−water interfaces (i.e., insular air bubbles) affect maximum colloid surface coverages in a manner similar to those acting near solid−water interfaces.

Best-fit estimates of k_2, the rate constant for air−water interface capture, vary between 0.16 and 0.49 h^{-1}, which translates to time scales for colloid immobilization (k_2^{-1}) at the outset of the experiments (when colloid concentrations at air−water interfaces were very low) ranging from 6 to 2 h. The magnitude of k_2 depends on the rate of colloid transport from the bulk fluid phase to the interface as well as on the probability that a particle collision with the interface will succeed in attachment. All of our experiments were conducted under identical chemical conditions; therefore, the attachment probability was constant across experimental treatments, and changes in k_2 reflect changes in system properties that influenced the rate at which particles struck the air−water interface. We find that k_2 decreases with Θ and, for experiments conducted at the same target Θ, that k_2 is lower for the imbibing-type experiments where the porewater velocities were lower. Analysis of the optimal parameters derived from both the imbibing- and drying-type experiments demonstrates that the magnitude of k_2 is proportional to the one-third power of the average porewater velocity (v). Filtration theory, derived to describe deposition of Brownian particles onto solid collectors within saturated packed beds, predicts the same functional dependence between the mass-transfer rate constant and the porewater velocity (*35*, *36*). This agreement between filtration theory-based predictions and our observations may be merely coincidental, but it does suggest that the single-collector model of filtration theory could be adapted to account for air−water interface mass transfer by treating insular air bubbles trapped within the pores as the collectors for colloid deposition. Development of this approach ultimately relies on advances in theory related to particle motion near curved air−water interfaces in porous media and on more realistic pore-scale models for air-phase geometry in natural media.

Our experimental results demonstrate that, under system conditions limiting colloid retention at the solid−water

interface, the transport of silica colloids through unsaturated media can be very efficient, even under low levels of water saturation. Comparison of our findings to those from research in saturated media (e.g., refs *7* and *31*) suggests that mass-transfer reactions at solid−water interfaces may be more effective in immobilizing mineral colloids than mass-transfer reactions that arise from the presence of the air phase. Nevertheless, mass-transfer reactions with the air phase measurably influence porewater colloid concentrations and will have to be represented in mathematical models for accurate prediction of colloid fluxes and colloid-bound contaminant fluxes within vadose-zone environments. Published studies have shown that single rate-law formulations successfully describe the air-phase-induced mass transfer of viruses and bacteria (*16*, *21*, *22*); however, perhaps due to differences in density and surface charge characteristics between silica colloids and the biocolloids, these single rate-law formulations are not fully capable of describing mass-transfer kinetics in our column experiments. We find that a dual rate-law model that incorporates a first-order rate law to simulate film straining and a second-order rate law to simulate capture at the air−water interfaces mimics the breakthrough data on silica transport very closely. This research represents an early step in the development of a comprehensive model for inorganic colloid transport in the vadose zone and forms a basis from which to explore more complex scenarios. We recommend that the experimental and theoretical work presented here be extended to incrementally account for complexities associated with a chemically reactive media and transients in porewater flow.

Acknowledgments

The work reported here was supported by the Hydrological Sciences Program of the National Science Foundation through Grant EAR-990958. We are thankful for the helpful comments provided by three anonymous reviewers.

Literature Cited

(1) El-Farhan, Y. H.; Denovio, N. M.; Herman, J. S.; Hornberger, G. M. *Environ. Sci. Technol.* **2000**, *34*, 3555−3559.
(2) Kaplan, D. I.; Bertsch, P. M.; Adriano, D. C.; Miller, W. P. *Environ. Sci. Technol.* **1993**, *27*, 1193−1200.
(3) Pilgrim, D. H.; Huff, D. D. *Earth Surf. Processes Landforms* **1983**, *8*, 451−463.
(4) Ryan, J. N.; Illangasekare, T. H.; Litaor, M. I.; Shannon, R. *Environ. Sci. Technol.* **1998**, *32*, 476−482.
(5) Seaman, J. C.; Bertsch, P. M.; Miller, W. P. *Environ. Sci. Technol.* **1995**, *29*, 1808−1815.
(6) Grolimund, D.; Borkovec, M.; Bartmettler, K.; Sticher, H. *Environ. Sci. Technol.* **1996**, *30*, 3118−3123.
(7) Saiers, J. E.; Hornberger, G. M. *Water Resour. Res.* **1996**, *32*, 33−41.
(8) McCarthy, J. F.; Zachara, J. M. *Environ. Sci. Technol.* **1989**, *23*, 496−502.
(9) Honeyman, B. D. *Nature* **1999**, *397*, 23−24.
(10) McDowell-Boyer, L. *Environ. Sci. Technol.* **1992**, *26*, 586−593.
(11) Ryan, J. N.; Elimelech, M. *Colloids Surf. A* **1996**, *107*, 1−56.
(12) Grolimund, D.; Elimelech, M.; Borkovec, M.; Bartmettler, K.; Kretzschmar, R.; Sticher, H. *Environ. Sci. Technol.* **1998**, *32*, 3562−3569.
(13) Elimelech, M.; Nagai, M.; Ko, C.-H.; Ryan, J. N. *Environ. Sci. Technol.* **2000**, *34*, 2143−2148.
(14) Wan, J.; Wilson, J. L. *Water Resour. Res.* **1994**, *30*, 11−23.
(15) Wan, J.; Wilson, J. L. *Water Resour. Res.* **1994**, *30*, 857−864.
(16) Corapcioglu, M. Y.; Choi, H. *Water Resour. Res.* **1996**, *32*, 3437−3449.
(17) Wan, J.; Tokunaga, T. K. *Environ. Sci. Technol.* **1997**, *31*, 2413−2420.
(18) Hillel, D. *Environmental Soil Physics*; Academic Press: London, 1998.
(19) van Genuchten, M. T. *Soil Sci. Soc. Am. J.* **1980**, *44*, 892−898.
(20) Jewett, D. G.; Logan, B. E.; Arnold, R. G.; Bales, R. C. *J. Contam. Hydrol.* **1999**, *36*, 73−89.
(21) Chu, Y.; Jin, Y.; Flury, M.; Yates, M. V. *Water Resour. Res.* **2001**, *37*, 253−263.
(22) Schafer, A.; Ustohal, P.; Harms, H.; Stauffer, F.; Dracos, T.; Zehnder, A. J. B. *J. Contam. Hydrol.* **1998**, *33*, 149−169.
(23) Litton, G. M.; Olson, T. M. *Environ. Sci. Technol.* **1993**, *27*, 185−193.
(24) Kohler, M.; Curtis, G. P.; Kent, D. B.; Davis, J. A. *Water Resour. Res.* **1996**, *32*, 3539−3551.
(25) Eching, S. O.; Hopmans, J. W. *Soil Sci. Soc. Am. J.* **1993**, *57*, 1167−1175.
(26) Saiers, J. E.; Hornberger, G. M. *Water Resour. Res.* **1999**, *25*, 1713−1727.
(27) Tuller, M.; Or, D. *Water Resour. Res.* **2001**, *37*, 1257−1276.
(28) Iwamatsu, M.; Horii, K. *J. Colloid Interface Sci.* **1996**, *182*, 400−406.
(29) Hough, D. B.; White, L. R. *Adv. Colloid Interface Sci.* **1980**, *14*, 3−41.
(30) Adamson, A. W. *Physical Chemistry of Surfaces*, 5th ed; John Wiley and Sons: New York, 1990.
(31) Saiers, J. E.; Hornberger, G. M.; Liang, L. *Water Resour. Res.* **1994**, *30*, 2499−2506.
(32) Wan, J.; Wilson, J. L.; Kieft, T. L. *Appl. Environ. Microbiol.* **1994**, *60*, 509−516.
(33) Gvirtzman, H.; Roberts, P. V. *Water Resour. Res.* **1991**, *27*, 1165−1176.
(34) Ko, C.-H.; Elimelech, M. *Environ. Sci. Technol.* **2000**, *34*, 3681−3689.
(35) Logan, B. E.; Jewett, D. G.; Arnold, R. G.; Bouwer, E. J.; O'Melia, C. R. *J. Environ. Eng.* **1995**, *121*, 869−873.
(36) Yao, K.-M.; Habibian, M. T.; O'Melia, C. R. *Environ. Sci. Technol.* **1971**, *5*, 1105−1112.

Received for review May 23, 2001. Revised manuscript received September 17, 2001. Accepted November 8, 2001.

ES0109949